THE JOURNAL OF BIOLOGICAL CHEMISTRY
Vol. 280, No. 24, Issue of June 17, pp. 22831–22838, 2005

Printed in U.S.A.

The *N*-Acetyl-D-glucosaminylphosphatidylinositol De-*N*-acetylase of Glycosylphosphatidylinositol Biosynthesis Is a Zinc Metalloenzyme*[S]

Received for publication, March 3, 2005, and in revised form, March 28, 2005
Published, JBC Papers in Press, April 6, 2005, DOI 10.1074/jbc.M502402200

Michael D. Urbaniak, Arthur Crossman, Tunhan Chang, Terry K. Smith, Daan M. F. van Aalten‡, and Michael A. J. Ferguson§

From the Division of Biological Chemistry and Molecular Microbiology, Wellcome Trust Biocentre, The University of Dundee, DD1 5EH Dundee, Scotland, United Kingdom

The de-*N*-acetylation of *N*-acetyl-D-glucosaminylphosphatidylinositol (GlcNAc-PI) is the second step of mammalian and trypanosomal glycosylphosphatidylinositol biosynthesis. Glycosylphosphatidylinositol biosynthesis is essential for *Trypanosoma brucei*, the causative agent of African sleeping sickness, and GlcNAc-PI de-*N*-acetylase has previously been validated as a drug target. Inhibition of the trypanosome cell-free system and recombinant rat GlcNAc-PI de-*N*-acetylase by divalent metal cation chelators demonstrates that a tightly bound divalent metal cation is essential for activity. Reconstitution of metal-free GlcNAc-PI de-*N*-acetylase with divalent metal cations restores activity in the order Zn^{2+} > Cu^{2+} > Ni^{2+} > Co^{2+} > Mg^{2+}. Site-directed mutagenesis and homology modeling were used to identify active site residues and postulate a mechanism of action. The characterization of GlcNAc-PI de-*N*-acetylase as a zinc metalloenzyme will facilitate the rational design of anti-protozoan parasite drugs.

Glycosylphosphatidylinositol (GPI)[1] acts as a membrane anchor for a significant proportion of eukaryotic cell surface glycoproteins. The structure, biosynthesis, and function of GPI anchors and related molecules have been extensively reviewed (1–6). The basic conserved GPI core of $NH_2CH_2CH_2PO_4H$-6Manα1–2Manα1–6Manα1–4GlcNα1–6-D-*myo*-inositol-1-HPO_4-lipid is often further decorated with additional ethanolamine phosphate and carbohydrate groups in a species- and tissue-specific manner. Biosynthesis of GPI, which occurs in the endoplasmic reticulum, is initiated by the transfer of GlcNAc from UDP-GlcNAc to phosphatidylinositol (PI) to generate *N*-acetyl-D-glucosaminylphosphatidylinositol (GlcNAc-PI). In the second step of the pathway, GlcNAc-PI is de-*N*-acetylated by *N*-acetyl-D-glucosaminylphosphatidylinositol deacetylase (EC 3.1.1.69, GlcNAc-PI de-*N*-acetylase) to give D-glucosaminylphosphatidylinositol (GlcN-PI) (7). De-*N*-acetylation is a prerequisite for subsequent mannosylation of GlcN-PI that leads to mature GPI anchor precursors (8).

GPI-anchored proteins are particularly abundant in protozoan parasites such as *Trypanosoma brucei*, the causative agent of African sleeping sickness in humans and the related disease Nagana in cattle (1). Sleeping sickness is invariably fatal if untreated and affect upwards of 300,000 people each year. Current drugs are highly toxic and difficult to administer, leaving an urgent need for new therapeutic agents. Blood stream form *T. brucei* cells express $\sim 5 \times 10^6$ GPI-anchored variant surface glycoprotein homodimers that form a dense surface coat, protecting the parasite from the complement pathway of the host and undergoing antigenic variation to evade specific immune responses (9, 10). Disruption of GPI biosynthesis is fatal to the bloodstream form parasite in culture (11–13), and a conditional null mutant of the gene encoding the GlcNAc-PI de-*N*-acetylase in *T. brucei* (*TbGPI12*) has validated this enzyme as a drug target (11).

Mammalian and trypanosomal GlcNAc-PI de-*N*-acetylases have a single pass N-terminal transmembrane domain with the majority of the protein found on the cytoplasmic face of the endoplasmic reticulum (14). *T. brucei* GPI12 has been partially purified from *T. brucei* membranes after detergent solubilization (15), whereas rat GlcNAc-PI de-*N*-acetylase (rPIG-L) has been expressed in *Escherichia coli* and isolated as a complex with GroEL (16). The specificities of GlcNAc-PI de-*N*-acetylase enzymes from *T. brucei* and HeLa cells have been examined *in vitro* using substrate analogues (8, 17). The *T. brucei* enzyme has less stringent substrate specificity than the mammalian enzyme, allowing the design of substrate-based species-specific inhibitors (18–20). However, the GlcNAc-PI de-*N*-acetylases are not well characterized. No structural data are available, and the active site and mechanism of action have yet to be determined.

The crystal structures of two proteins with limited homology to the GlcNAc-PI de-*N*-acetylases have recently been reported (21–23). The crystal structure of MshB, a zinc-dependent D-*N*-acetylglucosamine α1-*O*-1-D-*myo*-inositol de-*N*-acetylase involved in mycothiol synthesis in *Mycobacterium tuberculosis*,

* This work was supported by Grant 071463 from the Wellcome Trust Program. The costs of publication of this article were defrayed in part by the payment of page charges. This article must therefore be hereby marked "*advertisement*" in accordance with 18 U.S.C. Section 1734 solely to indicate this fact.

[S] The on-line version of this article (available at http://www.jbc.org) contains Supplemental Tables S1–S3 and Figs. S1 and S2.

‡ Recipient of a Wellcome Trust Senior Fellowship and an EMBO Young Investigator Fellowship.

§ To whom correspondence should be addressed: Division of Biological Chemistry and Molecular Microbiology, The School of Life Sciences, The University of Dundee, DD1 5EH Dundee, Scotland, United Kingdom. Tel.: 44-1382-344219; Fax: 44-1382-245764; E-mail: m.a.j.ferguson@dundee.ac.uk.

[1] The abbreviations used are: GPI, glycosylphosphatidylinositol; WT, wild type; CHO, Chinese hamster ovary; ES-MS, electrospray mass spectrometry; ES-MS-MS, electrospray mass spectrometry-mass spectrometry; GFP, green fluorescent protein; EGFP, enhanced GFP; GlcNAc-PI, *N*-acetyl-D-glucosaminylphosphatidylinositol; GlcN-PI, D-glucosaminylphosphatidylinositol; GlcN-*I*-P-C18, D-GlcNα1–6-D-*myo*-inositol-1-HPO_4-octadecyl; HA, hemagglutinin; HPTLC, high performance thin layer chromatography; MshB, *M. tuberculosis* 1-D-*myo*-inositol 2-acetamido-2-deoxy-α-D-glycopyranoside de-*N*-acetylase; M2S2, PIG-L-deficient CHO cell line; PE, phycoerythrin; PI, phosphatidylinositol; 1,10-PO, 1,10-phenanthroline; 1,7-PO, 1,7-phenanthroline; r.f.u., relative fluorescence units; rPIG-L, rat GlcNAc-PI de-*N*-acetylase; TbGPI12, GlcNAc-PI de-*N*-acetylase in *T. brucei*.

revealed an unusual HPDD zinc binding motif in the proposed active site (22, 23). This motif is conserved in the GlcNAc-PI de-*N*-acetylases, despite the low level of overall sequence identity with MshB. The protein TT1542 from *Thermus thermophilus* of unknown function has 23% sequence identity to MshB and also contains the HPDD motif. The crystal structure of TT1542 revealed a tertiary structure similar to MshB, but no metal ion was observed in the putative active site (21).

Here, we report that mammalian and trypanosomal GlcNAc-PI de-*N*-acetylases are zinc metalloenzymes and identify the active site residues by site-directed mutagenesis and molecular modeling. A putative mechanism of action is proposed.

EXPERIMENTAL PROCEDURES

Materials—[9,10-^{3}H]Myristic acid (40.2 Ci/mmol), UDP-[6-^{3}H]GlcNAc (UDP-[^{3}H]GlcNAc, 20 Ci/mmol), and En^{3}Hance^{TM} were purchased from PerkinElmer Life Sciences. High performance liquid chromatography-grade solvents were purchased from BDH, and all of the other reagents were purchased from Sigma.

Semi-synthetic and Synthetic Substrates—The synthesis of D-GlcNα1–6-D-*myo*-inositol-1-HPO$_4$-octadecyl (GlcN-*I*-P-C18) has been described by Crossman *et al.* (24). The formation of semi-synthetic [^{3}H]myristate-labeled GlcNAc-PI was conducted as described by Milne *et al.* (15). *N*-Acetyl derivates of the above compounds were prepared as described previously (25). The identity and purity of the synthetic substrates were assessed by negative ion electrospray-mass spectrometry (ES-MS), and the concentration of stock solutions was determined by measurement of the inositol content by selected ion-monitoring gas chromatography-mass spectrometry (26).

High Performance Thin Layer Chromatography—Glycolipid standards and samples were applied to 10-cm aluminum-backed Silica Gel 60 and developed with chloroform/methanol/13 M ammonia/1 M ammonium acetate/water (180/140/9/9/23, v/v). Dried HPTLC plates were sprayed with En^{3}Hance, and radiolabeled components were visualized by fluorography at −70 °C using Kodak X-Omat AR-5 film with an intensifying screen.

Typanosome Cell-free System Assays—Bloodstream form *T. brucei* (variant MITat1.4) were isolated, and membranes (cell-free system) were prepared as described previously and stored at −80 °C (27). Trypanosome membranes (2×10^7 cell equivalents/assay) were washed twice in 10 ml of modified incorporation buffer (0.1 M NaHEPES, pH 7.4, 50 mM KCl, 0.1 mM 1-chloro-3-tosylamido-7-amino-2-heptanone, and 1 μg/ml leupeptin). Me_2SO, with or without inhibitor, was added to 1% v/v, and the membranes were sonicated briefly and incubated on ice for 10 min. The treated membranes were washed, resuspended in 2× incorporation buffer (with or without inhibitor) with 10 mM dithiothreitol, and added to dry UDP-[^{3}H]GlcNAc (1 μCi) and sonicated briefly and incubated at 30 °C for 1 h. Glycolipid products were recovered by extraction into a chloroform/methanol/water mixture (10:10:3), evaporated to dryness, partitioned between butan-1-ol and water (28), and analyzed by HPTLC.

Site-directed Mutagenesis—Rat *PIG-L*-FLAG was PCR-amplified from the plasmid pMEEB-*PIG-L*-FLAG (14) using a 5′ primer (5′-ATAGTAT*AAGCTT*CCGGCTATGGAAGTGGTGGGT-3′), incorporating a HindIII site (*italics*), and a 3′ primer (5′-TTCGATT*GCGGCCGC*TTACTTGTCATCGTCG-3′), incorporating a NotI site (*italics*). The PCR fragment was subcloned into pcDNA3.1(+) with HindIII and NotI to give the plasmid pcDNA-*rPIG-L*-WT. The plasmid pLew100-*TbGPI12-myc*, which contains a *TbGPI12* insert with a silenced internal HindIII site, has been described previously (11).

Point mutations of *rPIG-L*-FLAG and *TbGPI12* were made using mutagenic synthetic oligonucleotide primers[2] in the QuikChange procedure (Stratagene) with mutations screened by sequencing of the insert. Successful mutations of *rPIG-L*-FLAG were PCR-amplified using a 5′ primer (5′-ATAGTAT*AAGCTT*CCGGCTATGGAAGTGGTGGGT-3′) incorporating a HindIII site (*italics*) and a 3′ primer (5′-AATTAA*TGGATC*CCGTTCCTTGTCATCGTCGTC-3′) incorporating a BamHI site (*italics*). The PCR fragment was subcloned into pEGFP-N1 with HindIII and BamHI to give the plasmid pEGFP-*rPIG-L*. Successful mutations of *TbGPI12* were PCR-amplified using a 5′ primer (5′-AATTTA*AAGCTT*GCTATGCATGTTGCTTTG-3′) incorporating a HindIII site (*italics*) and a 3′ primer (5′-AATTAA*TGGATC*CCGTCCCTTGTCATCGTCGTCCTTGTAGTCTCGCGACAGGTCC-3′) incorporating a BamHI site (*italics*) and a C-terminal FLAG tag (*underlined*). The PCR fragment was subcloned into pEGFP-N1 (Clontech) with HindIII and BamHI to give the plasmid pEGFP-*TbGPI12*.

Functional Complementation—The reporter cell line CHO-K1 M2S2, defective in *PIG-L* and stably transfected to express human-CD55 and -CD59, has been described by Nakamura *et al.* (14). CHO-K1 M2S2 cells and their transfectants were cultured in Ham's F-12 medium supplemented with 10% fetal calf serum, 100 units of penicillin and streptomycin, and 0.2 mg/ml G418 at 37 °C with 5% CO_2, 100% humidity. For transient transfections, cells were grown to 60–70% confluence in 6-well plates, and the contents of one well were used per transfection. Cells were washed with phosphate-buffered saline and trypsin-EDTA-treated for 15 min, washed with Ham's F-12 medium supplemented with 20 mM NaHEPES, and resuspended in 0.8 ml of the same solution (~2×10^6 cells/ml). The cells were transferred to 4-mm cuvettes containing 20 μg of the appropriate plasmid in distilled water and electroporated at 260 V, 950 microfarads (Bio-Rad gene-pulser). Immediately after transfection, 0.8 ml of fetal calf serum was added and the contents of the cuvette were transferred into 2 ml of culture medium in a 6-well plate and cultured for 72 h. Cells were detached with 0.5 mM EDTA in phosphate-buffered saline, washed three times in 0.25% bovine serum albumin in phosphate-buffered saline, incubated with mouse anti-CD55 (100 μg/ml) for 0.5 h, washed three times in phosphate-buffered saline with 0.25% w/v bovine serum albumin, and then incubated with an anti-mouse-phycoerythrin (PE) conjugate (STAR12A, Serotec) for 30 min. Cells were washed additionally three times in phosphate-buffered saline with 0.25% w/v bovine serum albumin before flow cytometry analysis in FACS-Calibur instrument (BD Biosciences).

Expression of rPIG-L—The QuikChange procedure (Stratagene) was used to create a silent mutation that removed the internal XhoI site in *rPIG-L* using the primers 5′-CCACCTCTACACCGTCTTT**T**TCGAGATACATGAGCGT-3′ and 5′-ACGCTCATGTATCTCGA**A**AAGACGGTGTAGAGGTGG-3′ (mutation in *boldface*) to give the plasmid pMEEB-*rPIG-L*-FLAG-sXho. The DNA encoding residues 24–252 of rPIG-L was amplified by PCR from pMEEB-*rPIG-L*-FLAG-sXho using a 5′ primer (5′-AAAC*CCATGG*ATAAGGTTTTAGATTCAGCGGAACGAAT-3′) that incorporated an NcoI site (*italics*) and a six-residue N-terminal sequence (MDKVLD, *underlined*) and a 3′ primer (5′-TTTT*CTCGAG*TGCGTAATCAGGGACGTCATAAGGGTAGCCGAGCAACTGCAGC-3′) that incorporated a C-terminal HA tag (GYPYDVPDYA, *underlined*) and a XhoI site (*italics*). The PCR fragment was subcloned into pET-Blue-2 (Novagen) with NcoI and XhoI to give the plasmid pETB-*eN-rPIGL-HA*, which incorporated a hexahistidine tag to the C terminus of the open reading frame.

E. coli Tuner^{TM} (Novagen) transformed with pETB-*eN-rPIGL-HA* were grown in Luria-Bertani medium with 50 μg/ml carbenicillin at 37 °C until A_{600} = 0.5, induced with 200 μM isopropyl β-D-thiogalactopyranoside, and cultured for an additional 16 h at 21 °C. Cells were harvested by centrifugation at 4500 × *g* for 20 min at 4 °C, resuspended in 10 ml of buffer A (50 mM Tris-HCl, 200 mM NaCl, 10 mM β-mercaptoethanol, 0.06% *n*-octyl-β-D-glucopyranoside, 10% glycerol (v/v)) per liter, and incubated with lysozyme (1 mg/ml) on ice for 20 min. Cells were lysed at 30,000 p.s.i. (OneShot, Constant Cell Disruption Systems), the lysate was clarified by centrifugation at 30,000 × *g* for 20 min at 4 °C, and then insoluble materials were removed by centrifugation at 100,000 × *g* for 1 h at 4 °C. The supernatant was filtered through a 0.4 μM membrane, applied to a 1-ml column precharged with Ni^{2+} (HiTrap Chelating HP, Amersham Biosciences), washed with buffer A, eluted with a gradient of 0–250 mM imidazole in buffer A (BioCad Sprint), and collected in 1-ml fractions. Fractions containing eN-rPIG-L-HA were identified by SDS-PAGE and Western blotting using an anti-HA mouse primary and an anti-mouse-horseradish peroxidase-conjugated secondary-antibody detected by chemiluminescence. Pooled fractions were concentrated and washed in buffer A in a 10,000 molecular weight cut-off spin-concentration device (Vivascience) repeatedly to remove imidazole. The concentration of eN-rPIG-L-HA was determined by absorbance at 280 nm using a calculated $\epsilon = 3.803 \times 10^4\ cm^{-1}\ M^{-1}$.

Radioactive De-N-acetylase Assay—[9,10-^{3}H]Myristate-labeled GlcNAc-PI (0.2 nCi, 50 fmol) was dried under a nitrogen stream, and 2× incorporation buffer (20 μl), distilled H_2O (10 μl), and buffer A (10 μl) with or without 100 ng of recombinant protein were added. The solution was briefly vortexed, sonicated for 5 s, and incubated at 37 °C for 30 min. Glycolipids were partitioned into butan-1-ol and the solvents were removed *in vacuo*, and the products were analyzed by HPTLC and fluorography.

ES-MS-MS De-N-acetylase Assay—All of the buffers and solutions

[2] Details of the mutagenic primers are contained in Supplemental Tables S1 and S2.

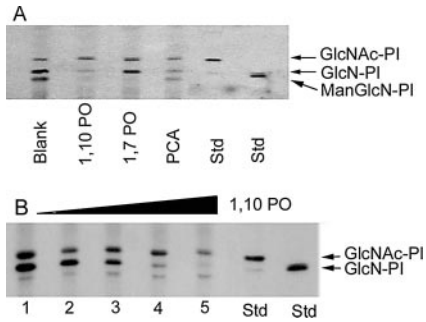

FIG. 1. **Effect of metal chelating agents on TbGPI12 activity in the trypanosome cell-free system.** *A*, the trypanosome cell-free system was labeled with UDP-[6-^{3}H]GlcNAc (*Blank*) or preincubated with 2.5 mM 1,10-phenanthroline (*1,10 PO*), 2.5 mM 1,7-phenanthroline (1,7-PO), or 2.5 mM 2,6-pyridinedicarboxylic acid (*PCA*) prior to labeling with UDP-[6-^{3}H]GlcNAc. Labeled glycolipids were extracted, partitioned into butan-1-ol, and analyzed by HPTLC and fluorography alongside [^{3}H]myristate-labeled GlcNAc-PI and GlcN-PI standards (*Std*). The *lower band* visible in some lanes is Manα1–4GlcN-PI. *B*, the effect of preincubation with increasing concentrations of 1,10-PO prior to labeling with UDP-[6-^{3}H]GlcNAc in the trypanosome cell-free system (0 mM (*lane 1*), 0.1 mM (*lane 2*), 0.5 mM (*lane 3*), 1.0 mM (*lane 4*), and 2.5 mM (*lane 5*)).

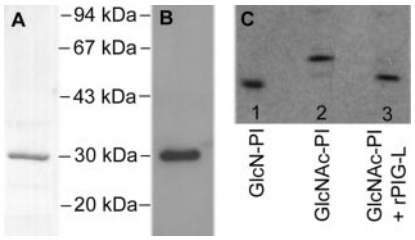

FIG. 2. **Expression of soluble rPIG-L.** *A*, 10% SDS-PAGE of the 28-kDa fusion protein eN-rPIG-L-HA stained with Coomassie Brilliant Blue R250. *B*, Western blot of eN-rPIG-L-HA detected with anti-HA primary antibody and a horseradish peroxidase-conjugated secondary antibody. *C*, GlcNAc-PI de-*N*-acetylase activity assay. [^{3}H]myristate-labeled GlcNAc-PI was treated with eN-rPIG-L-HA, and glycolipids were partitioned into butan-1-ol and analyzed by HPTLC and fluorography (*lane 3*) alongside [^{3}H]myristate-labeled GlcN-PI and GlcNAc-PI standards (*lanes 1* and *2*).

were treated with Chelex100 (sodium form) to remove divalent cations prior to use. The recombinant protein eN-rPIG-L-HA (500 ng/μl) was incubated with 1.0 mM 1,10-phenanthroline (1,10-PO) in buffer A for 0.5 h at 37 °C. Treated eN-rPIG-L-HA (1 μl) was added to GlcN-*I*-P-C18 (1 nmol) in incorporation buffer (39 μl) with or without 10 μM divalent metal cations. The solution was briefly vortexed, sonicated for 5 s, and incubated at 37 °C for 0.5 h. The mixture was diluted with 5% propan-1-ol (1 ml), the glycolipids were bound to C8 resin (100-mg Isolute cartridge), washed (5% propan-1-ol, 5 mM NH_4OAc), and eluted (60% propanol, 5 mM NH_4OAc), and the products were analyzed directly by ES-MS-MS on a Micromass Quattro Ultima triple quadrupole mass spectrometer in parent ion-scanning mode (parents of *m/z* 233). The *m/z* 233 fragment ion, [inositol-1,2-cyclic phosphate-H_2O], is common to both the GlcNAc-*I*-P-C18 substrate and the GlcN-*I*-P-C18 product. The ratio of the integrals for the *m/z* 714 [GlcNAc-*I*-P-C18-H] and *m/z* 672 [GlcN-*I*-P-C18-H] parent ions was used to calculate the percentage of substrate conversion to product in a given sample.

Molecular Modeling—A structural model of rPIG-L was constructed using homology modeling with WHAT IF (29). The structure of *M. tuberculosis* MshB (Protein Data Bank entry 1Q7T (23)) was used as the template structure. No attempt was made to model the large insertions in the rPIG-L sequence (Fig. 8). Rotamers of conserved residues were left unchanged. All of the other residues were initially mutated to alanines. Rotamers were then modeled using the WHAT IF backbone-dependent rotamer libraries. At each position, rotamer quality was checked by hydrogen bonding, van der Waals bumps, and packing quality. The coordinates for the zinc ion and a water molecule coordinated by the zinc ion were obtained by superposition with the apoMshB structure (Protein Data Bank entry 1Q74 (22)). Pictures were made with PyMol (30) and GRASP (31).

RESULTS

Typanosome Cell-free System Assays—The trypanosome cell-free system converts UDP-[6-^{3}H]GlcNAc to [6-^{3}H]GlcNAc-PI, which is de-*N*-acetylated by TbGPI12 to give [6-^{3}H]GlcN-PI, which may then be partially converted to Manα1–4GlcN-PI and later GPI intermediates at the expense of traces of endogenous Dol-P-Man in the cell-free system membrane (Fig. 1*A*, *blank*) (32). In order to investigate the metal dependence of TbGPI12, we examined the ability of the trypanosome cell-free system to de-*N*-acetylate GlcNAc-PI in the presence of divalent metal cation-chelating agents. 1,10-PO chelates Zn^{2+}, $Ni^{2+} \gg Mn^{2+}$, Mg^{2+}, whereas the isomeric 1,7-phenanthroline (1,7-PO) is unable to chelate metal ions, and 2,6-pyridinedicarboxylic acid has affinity for a broad range of divalent metal cations (33). Prewashing the cell-free system to remove any loosely associated divalent metal ion did not affect the de-*N*-acetlyase activity. However, preincubation of the cell-free system with 1,10-PO or pyridinedicarboxylic acid inhibits de-*N*-acetylation, whereas the non-chelating 1,7-PO has no effect (Fig. 1*A*). Inhibition by 1,10-PO occurs in a concentration-dependent manner (Fig. 1*B*), suggesting the presence of a strongly bound metal ion that is essential for TbGPI12 activity.

Expression of Soluble rPIG-L—Truncation of the N-terminal transmembrane domain of rPIG-L at residues 7, 14, and 21–27 failed to produce soluble recombinant rPIG-L in *E. coli*. A BLAST search with rPIG-L revealed a hypothetical *E. coli* protein YAIS with reasonable homology to rPIG-L[3] but lacking the transmembrane domain. A pET vector pETB-*eN-rPIG-L-HA* was constructed, coding for a 28-kDa fusion protein eN-rPIG-L-HA comprising residues 1–6 of *E. coli* YAIS followed by residues 26–252 of rPIG-L and C-terminal HA and hexahistidine tags. The expression in *E. coli* and purification by metal ion affinity chromatography produced soluble eN-rPIG-L-HA (Fig. 2*A*). The identity of the protein was confirmed by Western blotting with anti-HA (Fig. 2*B*) and by tryptic peptide mass fingerprinting.[4]

Metal Ion Dependence of Soluble rPIG-L—Initial assessment of the activity of eN-rPIG-L-HA by measuring the de-*N*-acetylation of [H^3]myristate-labeled GlcNAc-PI confirmed that the fusion protein retained activity for its natural substrate (Fig. 2*C*, *lane 3*). To provide quantitative data and enable higher substrate concentrations to be used, a ES-MS-MS technique was devised to monitor the de-*N*-acetylation of the synthetic substrate GlcNAc-*I*-P-C18 (see "Experimental Procedures"). Although GlcNAc-*I*-P-C18 has been reported to be a poorer substrate than GlcNAc-PI in the HeLa cell-free system where the enzyme is membrane-bound (34), a specific activity of 2.3 μmol/mg/h was recorded. This figure compares favorably with the previously reported specific activity of 390 pmol/mg/h for the de-*N*-acetylation of GlcNAc-PI by partially purified TbGPI12 from *T. brucei* (15).

The activity of eN-rPIG-L-HA was inhibited by the presence of micromolar concentrations of Zn^{2+} (IC_{50} 35 μM), a feature previously observed for several Zn^{2+} metalloenzymes (35, 36). Incubation of eN-rPIG-L-HA with 1,10-PO produced a loss of de-*N*-acetylase activity in a time- and concentration-dependent manner, such that treatment with 2.5 mM 1,10-PO for 1 h at 37 °C was sufficient to completely remove all activity. Attempts were made to restore activity to the metal-free inactive protein (apo-eN-rPIG-L-HA) by reconstitution with a variety of metal

[3] The alignment of rat PIG-L and *E. coli* YAIS is contained in Supplemental Fig. S2.

[4] Details of the tryptic peptide mass fingerprinting of eN-rPIG-L-HA is contained in Supplemental Table S3.

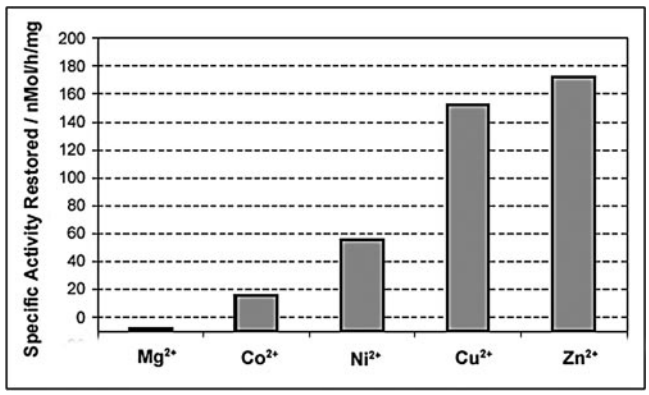

FIG. 3. **Addition of metal ions increases the activity of apo-rPIG-L.** Apo-rPIG-L was produced by incubation of eN-rPIG-L-HA with 1.0 mM 1,10-PO for 30 min at 37 °C. The specific activity of apo-eN-rPIG-L-HA was measured using the ES-MS-MS de-*N*-acetylase assay in the presence or absence of 10 μM divalent metal cations.

ions without success. However, under less harsh conditions where partially active apo-eN-rPIG-L-HA was obtained, the activity could be increased by the addition of divalent metal cations. Furthermore, the lower the activity of the apo-eN-rPIG-L-HA sample, the less the activity could be restored. As an example, treatment of eN-rPIG-L-HA with 1.0 mM 1,10-PO for 30 min at 37 °C produced a 83% loss in activity that could be partially restored (to a maximum of 28%) by the subsequent addition of metal ions (10 μM) with restoration occurring in the order Zn^{2+}, $Cu^{2+} > Ni^{2+} > Co^{2+} > Mg^{2+}$ (Fig. 3). The addition of 10 μM of the same metal ions to untreated eN-rPIG-L-HA had a negligible effect on its de-*N*-acetylase activity (with the exception of zinc, which showed 40% inhibition). These results indicate that apo-eN-rPIG-L-HA is unstable, probably undergoing irreversible misfolding. The amount of de-*N*-acetylase activity that can be reconstituted appears to be a balance between the rate of metal ion stripping and the instability of apo-eN-rPIG-L-HA.

Site-directed Mutagenesis—Sequence alignment of the GlcNAc-PI de-*N*-acetylase enzymes from *T. brucei* and *Rattus norvegicus* with MshB from *M. tuberculosis* revealed a number of conserved residues, despite their low level of sequence identity (Fig. 4). Many, but not all, of these residues are also completely conserved in putative GlcNAc-PI de-*N*-acetylase homologues that are identified in a number of sequenced eukaryotic genomes (see Fig. 4, *consensus line*). The sequence alignment was used to construct a homology model of the rPIG-L active site (Fig. 8). The sequence alignment and model show that a large proportion of the conserved residues are found in the proposed active site, including the putative zinc-binding residues and catalytic base (22, 23). Site-directed mutagenesis was used to mutate 14 rPIG-L residues to alanine, covering the zinc-binding residues and other residues proposed to participate in catalysis or substrate binding (Fig. 4). The *rPIG-L* mutants were cloned into pEGFP mammalian expression vector, which fused GFP to the C terminus of the protein.

Establishment of a Semi-quantitative Complementation Assay—The reporter cell line CHO-K1 M2S2, defective in PIG-L and stably transfected to express two human GPI-anchored proteins (CD55 and CD59), has been used previously to assess the activity of potential GlcNAc-PI de-*N*-acetylases by functional complementation (11, 14, 16). Transfection of the M2S2 cell line with a vector expressing functional GlcNAc-PI de-*N*-acetylase restores GPI biosynthesis and thus cell surface expression of CD55 and CD59, which can be detected by immunofluorescence. To correlate the level of de-*N*-acetylase activity with the level of protein expression, we cloned *rPIG-L* into pEGFP mammalian expression vector, which fused GFP to the C terminus of the expressed protein. CHO-K1 M2S2 cells were transiently transfected with various recombinant plasmids, and the level of GFP expression and cell surface restoration of CD55 was analyzed by flow cytometry (Fig. 5).

Transfection with pcDNA-*rPIG-L* expressing wild type rPIG-L restored cell surface expression of CD55 (defined as a PE signal $\geq 10^2$ relative fluorescence units (r.f.u.), CD55-positive) with no GFP signal (Fig. 5*A*), whereas transfection with empty pEGFP expressing EGFP produced a GFP signal (defined as a GFP signal $\geq 10^1$ r.f.u, GFP-positive) with no CD55 restoration (Fig. 5*B*). Transfection with pEGFP-*rPIG-L*-WT expressing the rPIG-L-WT-GFP fusion restored cell surface expression of CD55 with CD55-positive cells showing varying levels of GFP signal (Fig. 5*C*). These results indicate that, for wild type rPIG-L enzyme at least, cell surface restoration of CD55 is effectively complete in transfected cells, whereas the GFP signal varies continuously depending on the level of protein expression in individual cells. The fact that full CD55 restoration can be achieved in transfectants expressing undetectable amounts of GFP suggests that the amount of rPIG-L required to complement the M2S2 mutant cell line is extremely small.

Analysis of rPIG-L Mutants by Functional Complementation—To compare the activity of the rPIG-L alanine mutants, M2S2 cells were transiently transfected with plasmids expressing various rPIG-L-GFP fusion proteins and the level of GFP expression and cell surface restoration of CD55 was analyzed by flow cytometry (Table I). The activity of the rPIG-L mutants was compared by measuring the mean GFP signal of CD55-positive cells, allowing the rPIG-L mutants to be grouped into three distinct classes defined as follows: (i) those with activities similar to wild type rPIG-L with a mean GFP signal of 3–17 r.f.u. (+ class, Fig. 6*A*); (ii) those with negligible activities compared with wild type rPIG-L with a mean GFP signal of $>10^2$ r.f.u. (− class, Fig. 6*B*); and (iii) those that display activity only when a GFP signal is detected with a mean GFP signal of 20–35 r.f.u. (± class, Fig. 6*C*).

Two mutants in the + class, D147A and H226A, displayed lower GFP signals than the wild type enzyme (Fig. 6*D*), which may reflect poor folding of these mutants, because the level of fluorescence of GFP fusions has been related to the stability of the upstream protein (37). However, the level of rPIG-L activity of these mutants is still sufficient to completely restore cell surface expression of CD55. The − class mutants produce incomplete cell surface restoration of CD55, even at very high levels of rPIG-L-GFP expression, indicating that the mutation has severely reduced the activity of the enzyme. In contrast, the ± class mutants are able to completely restore cell surface expression of CD55, but only as the levels of rPIG-L-GFP expression increases, indicating that the mutation has only a minor detrimental effect on the activity of the enzyme.

Analysis of TbGPI12 Wild Type and Alanine Mutants by Functional Complementation—TbGPI12 wild type was cloned into the pEGFP to give the plasmid pEGFP-*TBGPI12-WT* and transiently transfected into CHO-K1 M2S2 cells. Flow cytometry analysis showed that the TbGPI12-GFP fusion fully restored cell surface expression of CD55 but failed to produce the range of GFP signals observed for the rPIG-L-GFP fusion (data not shown). The low GFP signal for TbGPI12-GFP, similar to that seen for rPIG-L-GFP mutants D147A and H226A (Fig. 6*D*), presumably reflects a lower level of protein stability and/or expression than rPIG-L-GFP wild type (37).

Site-directed mutagenesis was used to mutate the three putative zinc-binding residues of *TbGPI12* to alanine (Fig. 4). The *TbGPI12* mutants were cloned into pEGFP, transiently trans-

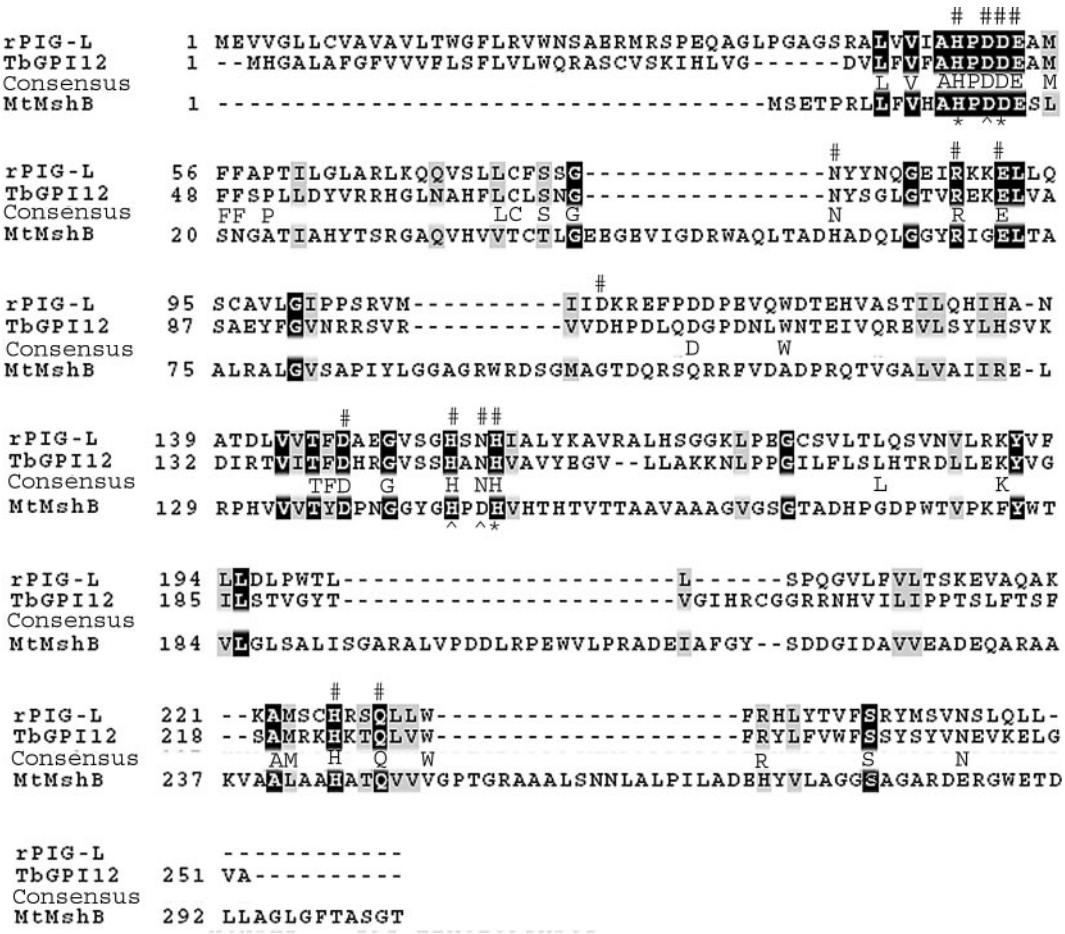

FIG. 4. **Sequence alignment of GlcNAc-PI de-*N*-acetylases with MshB.** The sequences are from *R. norvegicus* (rPIG-L), *T. brucei* (TbGPI12), and *M. tuberculosis* (MtMshB). The *consensus line* gives residues that are totally conserved in known or putative GlcNAc-PI de-*N*-acetylases from *Homo sapien*, *Cannis familiaris*, *Mus musculus*, *R. norvegicus*, *Anopheles gambiae*, *Drosophila melanogaster*, *T. brucei*, *Cryptococcus neoformans*, *Leishmania major*, *Arabidopsis thaliana*, and *Schizosaccharomyces pombe* (the alignment of the GlcNAc-PI de-*N*-acetylases used to create the consensus sequence is contained in the supplemental data). Conserved residues are highlighted in *black* (identical) or *gray* (similar). *, proposed zinc-binding residues; ^, proposed catalytic residues; #, alanine point mutations of rPIG-L. Alignment was created by T-Coffee (40).

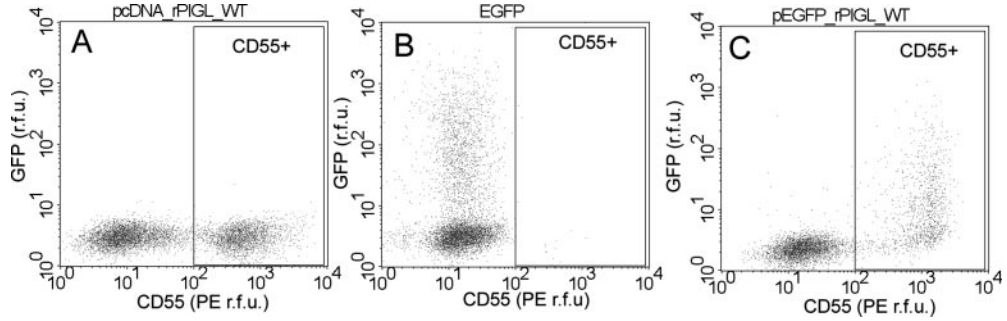

FIG. 5. **Flow cytometry analysis of transiently transfected CHO-K1 M2S2 cells.** The CHO-K1 M2S2 cell line was defective in PIG-L and failed to display GPI-anchored proteins on the cell surface. *A*, transfection with pcDNA-*rPIG-L*-WT, which expresses rPIG-L, restored cell surface expression of the GPI-anchored protein human CD55 detected by immunofluorescence using a mouse anti-CD55 primary antibody and anti-mouse-PE-conjugated secondary antibody. CD55-positive (*CD55+*, *boxed area*) cells are defined as having a PE signal $\geq 10^2$ r.f.u. Untransfected cells (*bottom left corner*) gave no signal. *B*, transfection with pEGFP produced a GFP signal directly proportional to the level of protein expression where GFP-positive cells are defined as having a GFP signal $\geq 10^1$ r.f.u. *C*, transfection with an pEGFP-*rPIG-L*-WT, which expresses an rPIG-L-GFP fusion protein, produced cell surface restoration of CD55 and a GFP signal proportional to the level of protein expression.

fected into CHO-K1 M2S2 cells, and analyzed by flow cytometry. To allow the comparison of the activities of the TbGPI12 mutants, successfully transfected cells were selected for analysis by considering only those cells with a GFP signal $\geq 10^1$ r.f.u (Fig. 7). As expected, transient transfection with pEGFP produced no CD55-positive cells (Fig. 7*A*), pcDNA-*rPIG-L*, having no GFP signal, gave no cell count at all (Fig. 7*B*), and pEGFP-*TbGPI12-WT* gave 93.2% CD55-positive cells. The TbGPI12 mutants gave significantly decreased the levels of de-*N*-acetylase activity, pEGFP-*TbGPI12-H41A* gave 9.2% CD55-positive cells (Fig. 7*D*), pEGFP-*TbGPI12-D44A* gave 0.8% CD55-positive cells (Fig. 7*E*), and pEGFP-*TbGPI12-H150A* gave 34.5% CD55-positive cells (Fig. 5*F*). The relative severity of the mutations on the apparent de-*N*-acetylase activity was the same as that for the corresponding putative zinc-binding residues in rPIG-L (Table I).

TABLE I
Flow cytometry analysis of M2S2 CHO-K1 cells transiently transfected with plasmids expressing GFP fusions of rPIG-L alanine mutants

Experimental details are as outlined in Fig. 5. + Class mutations produce cell surface restoration of the GPI-anchored protein, human CD55, and a GFP signal proportional to the level of protein expression. − Class mutations produce incomplete cell surface restoration of CD55, even at very high levels of protein expression. ± Class mutations produce complete cell surface restoration of CD55 when a GFP signal $\geq 10^1$ r.f.u is detected.

Mutant	Class	GFP signal[a]	Proposed role in MshB (22, 23)
WT		9.4	
H49A	−	154.6	Zinc coordination
D51A	−	>10,000[b]	Catalytic base
D52A	−	879.5	Zinc coordination
E53A	±	21.3	H-bonds to αNH of Asp^{51}
N80A	+	14.1	Maintaining active site geometry
R88A	±	27.0	Substrate binding
E91A	+	15.4	Maintaining active site geometry
D116A	+	13.6	Substrate binding
D147A	+[c]	3.2	Maintaining active site geometry
H154A	+	10.7	Proton donor (direct)
N156A	+	16.5	Proton donor (indirect)
H157A	±	32.1	Zinc coordination
H226A	+[c]	3.4	Maintaining active site geometry
Q229A	+	11.4	Substrate binding

[a] Average GFP signal of cells showing cell surface restoration of CD55. CD55-positive cells are defined as having a PE signal $\geq 10^2$ r.f.u.
[b] No CD55-positive cells were detected at any level of GFP expression.
[c] GFP signal observed was lower than wild type.

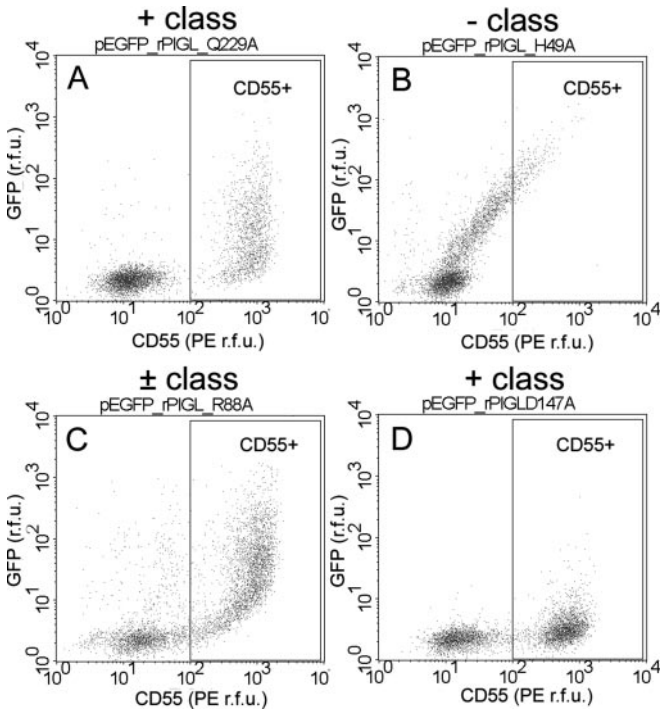

FIG. 6. **Flow cytometry analysis of M2S2 CHO-K1 cells transiently transfected with plasmids expressing GFP fusions of rPIG-L alanine mutants.** Experimental details are as outlined in Fig. 5. Data representative of the classes defined in the text are shown. *A*, + *class*, pEGFP-*rPIG-L-Q229A* produced cell surface restoration of the GPI-anchored protein human CD55 and a GFP signal proportional to the level of protein expression. Untransfected cells (*bottom left corner*) gave no signal. *B*, − *class*, pEGFP-*rPIG-L-H49A* produced incomplete cell surface restoration of CD55, even at very high levels of protein expression. *C*, ± *class*, pEGFP-*rPIG-L-R88A* produced complete cell surface restoration of CD55 only when a GFP signal $\geq 10^1$ r.f.u was detected. *D*, + class with low GFP signal. pEGFP-*rPIG-L-D147A* produced complete cell surface restoration of CD55 but with a mean GFP signal significantly lower than that for the wild type rPIG-L-GFP fusion.

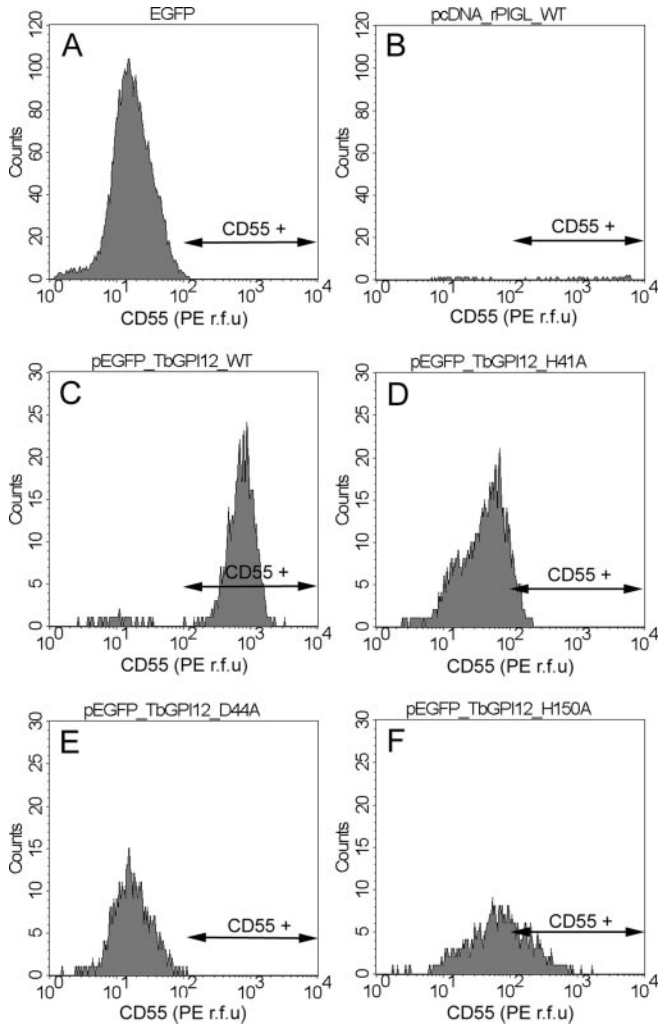

FIG. 7. **Flow cytometry analysis of M2S2 CHO-K1 cells transiently transfected with plasmids expressing GFP fusions of TbGPI12 alanine mutants.** Experimental details are as outlined in Fig. 5. Successfully transfected cells were selected for analysis by considering only those cells with a GFP signal $\geq 10^1$ r.f.u. CD55-positive cells have a PE signal $>10^2$ r.f.u and are indicated on the graph by a *double-headed arrow* labeled CD55+. Transient transfections are noted as follows: the GFP-positive control pEGFP expressing GFP gave no CD55-positive cells (*A*); the CD55-positive control pcDNA-*rPIG-L* expressing no GFP gave no cell count (*B*); pEGFP-*TbGPI12-WT* expressing TbGPI12-WT-GFP gave 93.2% CD55-positive cells (*C*); pEGFP-*TbGPI12-H41A* expressing TbGPI12-H41A-GFP gave 9.2% CD55-positive cells (*D*); pEGFP-*TbGPI12-D44A* expressing TbGPI12-D44A-GFP gave 0.8% CD55-positive cells (*E*); and pEGFP-*TbGPI12-H150A* expressing TbGPI12-H150A-GFP gave 34.5% CD55-positive cells (*F*).

DISCUSSION

We have demonstrated that the mammalian and trypanosomal GlcNAc-PI de-*N*-acetylases require the presence of a strongly bound divalent metal cation for activity. We propose that native GlcNAc-PI de-*N*-acetylases contain zinc at the active site, because they contain a conserved zinc binding motif (Fig. 4) (22, 23) and are inhibited by micromolar concentrations of Zn^{2+} (characteristic of zinc metalloproteins (35)) and because Zn^{2+} is most effective in reconstituting enzymatic activity in the apoprotein (Fig. 3).

Analysis of the mutagenesis data in the context of the rPIG-L model reveals that there are essentially four types of conserved residues in the GlcNAc-PI de-*N*-acetylases. The first group of residues directly coordinates the zinc ion, His^{49}, Asp^{52}, and His^{157}, which form a classic zinc-binding triad. Although the H49A and D52A have large effects on activity (Table I), the

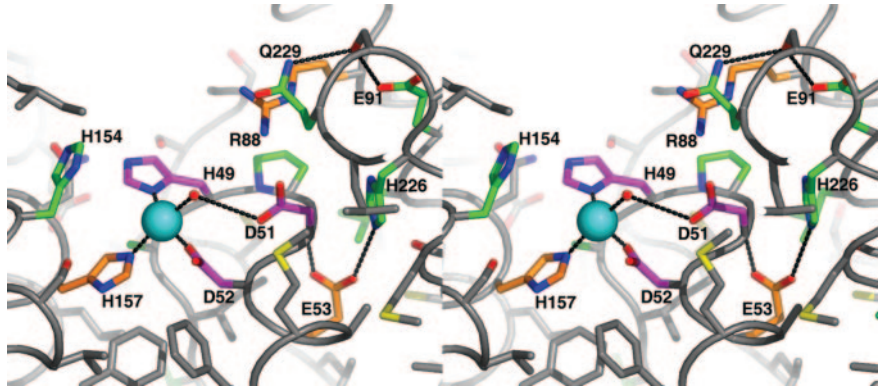

FIG. 8. **Molecular model of rPIG-L active site.** The rPIG-L active site was modeled with WHAT IF (29) using MshB (Protein Data Bank entry 1Q7T (23)) as the template. Stereoview of rPIG-L active site is shown with conserved residues colored as follows. Oxygen atoms are colored *red*. Sulfur atoms are colored *yellow*. Carbon atom coloring denotes the role of the residues as follows: *magenta*, − class residues essential for activity; *orange*, ± class residues important for activity; *green*, + class residues with no effect on activity. Zinc is colored *light blue*, hydrogen bonds are represented as *dashed lines*, main chain backbone atoms are represented as a C_α trace in *gray*.

H157A mutation only has an intermediate effect. The model shows that His^{49} and Asp^{52} are close to the proposed catalytic base, Asp^{51} (Fig. 8), whereas His^{157} occupies a position on the far side of the active site. Furthermore, His^{154} may be positioned sufficiently closely to be able to replace the zinc-binding role of His^{157} with minimal structural rearrangement.

The second group of residues are those involved in catalysis and/or substrate binding and directly line the active site cleft. Asp^{51} occupies a position near the zinc ion but does not interact with it directly. Rather, as seen in one of the MshB crystal structures (Protein Data Bank entry 1Q74 (22)), it appears to coordinate a water molecule bound to zinc (Fig. 8). The fact that this is the only mutation that produces no detectable activity but is not involved in zinc coordination suggests that this may be the catalytic base, activating a water molecule for attack on the acetamidocarbonyl carbon. A conserved histidine, His^{154}, is positioned opposite this water molecule (Fig. 8) and could be involved in the coordination and polarization of the acetamido group as observed in several other de-*N*-acetylases (22, 38). However, the mutation of this histidine has no significant effect (Table I). There are two further conserved residues lining the active site, Arg^{88} and Gln^{229}. These are too distant from the catalytic center to be involved in the reaction mechanism and have previously been proposed to participate in substrate binding (23). Mutation of these residues show weak or intermediate effects (Table I).

The third group of residues are those in a second shell of conservation buried behind active site residues. Glu^{53}, Glu^{91}, and His^{226} are all buried and coordinate residues from the second group by hydrogen bonding (Fig. 8). Being further away from the active site, mutations of these residues have almost no detectable effect on activity.

The fourth group consists of conserved residues far away from the active site (beyond the area shown in Fig. 8). These are mostly conserved hydrophobic residues involved in packing the core of the enzyme with the exception of Asn^{80}, Asp^{116}, and Asp^{147}, which are solvent-exposed and overall do not show significant effects on mutation.

Given the apparent similarity of the active site of the GlcNAc-PI de-*N*-acetylase with that of MshB and zinc metalloproteinases, we are able to postulate a putative catalytic mechanism consistent with our experimental observations (Fig. 9). In this mechanism, the acetamidocarbonyl oxygen of GlcNAc-PI binds directly to zinc ion, polarizing the carbonyl bond and leaving a partial positive charge on the carbon atom. Nucleophilic attack of a zinc-bound water molecule activated by the general base Asp^{51} forms a tetrahedral intermediate stabilized by coordination to zinc. Subsequent protonation by Asp^{51} or His^{154} in a non-rate-limiting step allows the loss of GlcN-PI with displacement of the zinc-bound acetate by an incoming water molecule completing the catalytic cycle.

In summary, we have identified the active site residues of

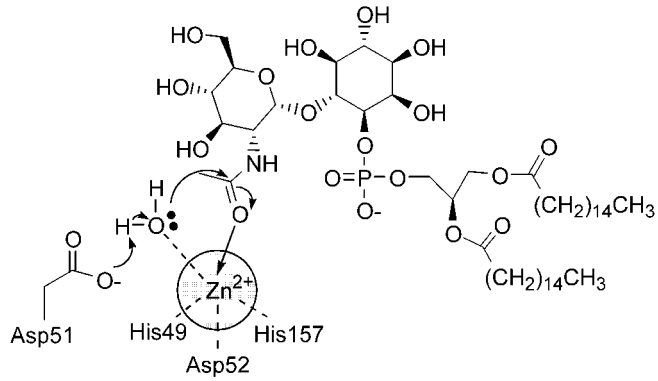

FIG. 9. **Putative mechanism of action of the GlcNAc-PI de-*N*-acetylases.** In this model, the catalytic base Asp^{51} assists the nucleophilic attack of a zinc-bound water molecule on the activated acetamidocarbonyl with subsequent protonation of the tetrahedral intermediate promoting loss of acetic acid. Residues numbering is based on rPIG-L

the GlcNAc-PI de-*N*-acetylases and postulated a catalytic mechanism. The GlcNAc-PI de-*N*-acetylase of *T. brucei*, the causative agent of African sleeping sickness, has been genetically validated as a drug target (11), and parasite-specific inhibitors of the enzyme have been designed and synthesized (19). Our characterization of the GlcNAc-PI de-*N*-acetylases as zinc metalloenzymes will facilitate further rational design of inhibitors and potential drug leads, because the pharmacology of inhibiting zinc metalloenzymes is well established (39).

Acknowledgments—We thank Rosemary Clarke for assistance with flow cytometry, Yusuke Maeda for tips on transfecting CHO cells, and M. Lucia S. Guther for providing *T. brucei* cell-free system. We are grateful to Taroh Kinoshita for providing the M2S2 CHO-K1 cell line, B. Paul Morgan for the anti-CD55 monoclonal antibody, and John S. Brimacombe for continued interest. We thank Christian R. H. Raetz and Robert C. Fahey for useful discussions.

REFERENCES

1. Ferguson, M. A. J. (1999) *J. Cell Sci.* **112,** 2799–2809
2. Morita, Y. S., Acosta-Serrano, A., and Englund, P. T. (2000) in *Oligosaccharides in Chemistry and Biology-A Comprehensive Handbook* (Ernst, P. S., and Hart, G. W., eds) pp. 417–433, Wiley-VCH, Weinheim, Germany
3. Ferguson, M. A. J., Brimacombe, J. S., Brown, J. R., Crossman, A., Dix, A., Field, R. A., Guther, M. L. S., Milne, K. G., Sharma, D. K., and Smith, T. K. (1999) *Biochim. Biophys. Acta* **1455,** 327–340
4. Kinoshita, T., and Inoue, N. (2000) *Curr. Opin. Chem. Biol.* **4,** 632–638
5. Macedo, C. S. D., Shams-Eldin, H., Smith, T. K., Schwarz, R. T., and Azzouz, N. (2003) *Biochemie* **85,** 465–472
6. Eisenhaber, B., Maurer-Stroh, S., Novatchkova, M., Schneider, G., and Eisenhaber, F. (2003) *BioEssays* **25,** 367–385
7. Doering, T. L., Masterson, W. J., Englund, P. T., and Hart, G. W. (1989) *J. Biol. Chem.* **264,** 11168–11173
8. Sharma, D. K., Smith, T. K., Crossman, A., Brimacombe, J. S., and Ferguson, M. A. J. (1997) *Biochem. J.* **328,** 171–177
9. Cross, G. A. M. (1996) *BioEssays* **18,** 283–291
10. Mehlert, A., Zitzmann, N., Richardson, J. M., Traumann, A., and Ferguson, M. A. J. (1998) *Mol. Biochem. Parasitol.* **91,** 145–152
11. Chang, T., Milne, K. G., Guther, M. L. S., Smith, T. K., and Ferguson, M. A. J.

(2002) *J. Biol. Chem.* **277,** 50176–50182
12. Lillico, S., Field, M. C., Blundell, P., Coombs, G. H., and Mottram, J. C. (2003) *Mol. Biol. Cell* **14,** 1182–1194
13. Nagamune, K., Nozaki, T., Maeda, Y., Ohishi, K., Fukuma, T., Hara, T., Schwarz, R. T., Sutterlin, C., Brun, R., Reizman, H., and Kinoshita, T. (2000) *Proc. Natl. Acad. Sci. U. S. A.* **97,** 10336–10341
14. Nakamura, N., Inoue, N., Wantanabe, R., Takahashi, M., Takeda, J., Stevens, V. L., and Kinoshita, T. (1997) *J. Biol. Chem.* **272,** 15834–15840
15. Milne, K. G., Field, R. A., Masterson, W. J., Cottaz, S., Brimacombe, J. S., and Ferguson, M. J. (1994) *J. Biol. Chem.* **269,** 16403–16408
16. Wantabe, R., Ohishi, K., Maeda, Y., Nakamura, N., and Kinoshita, T. (1999) *Biochem. J.* **339,** 185–192
17. Sharma, D. K., Smith, T. K., Weller, C. T., Crossman, A., Brimacombe, J. S., and Ferguson, M. A. J. (1999) *Glycobiology* **9,** 415–422
18. Smith, T. K., Crossman, A., Brimacombe, J. S., and Ferguson, M. A. J. (2004) *EMBO J.* **23,** 4701–4708
19. Smith, T. K., Crossman, A., Borrissow, C. N., Paterson, M. J., Dix, A., Brimacombe, J. S., and Ferguson, M. A. J. (2001) *EMBO J.* **20,** 3322–3332
20. Smith, T. K., Patterson, M. J., Crossman, A., Brimacombe, J. S., and Ferguson, M. A. J. (2000) *Biochemistry* **39,** 11801–11807
21. Handa, N., Terada, T., Kamewari, Y., Hamana, H., Tame, J. R. H., Park, S.-Y., Kinoshita, K., Ota, M., Nakamura, H., Kuramitsu, S., Shirouzu, M., and Yokoyama, S. (2003) *Protein Sci.* **12,** 1621–1632
22. Maynes, J. T., Garen, C., Cherney, M. M., Newton, G., Arad, D., Av-Gay, Y., Fahey, R. C., and James, M. N. G. (2003) *J. Biol. Chem.* **278,** 47166–47170
23. McCarthy, A. A., Paterson, N. A., Knijff, R., and Baker, E. N. (2004) *J. Mol. Biol.* **335,** 1131–1141
24. Crossman, A., Patterson, M. J., Ferguson, M. A. J., Smith, T. K., and Brimacombe, J. S. (2002) *Carbohydr. Res.* **337,** 2049–2059
25. Smith, T. K., Cottaz, S., Brimacombe, J. S., and Ferguson, M. A. J. (1996) *J. Biol. Chem.* **271,** 6476–6482
26. Ferguson, M. A. J. (1994) in *Glycobiology: A Practical Approach* (Fukuda, M., and Kobata, A., eds) pp. 349–383, IRL Oxford University Press, Oxford
27. Masterson, W. J., Doering, T. L., Hart, G. W., and Englund, P. W. (1989) *Cell* **62,** 73–80
28. Guther, M. L. S., Masterson, W. J., and Ferguson, M. A. J. (1994) *J. Biol. Chem.* **269,** 18694–18701
29. Vriend, G. (1990) *J. Mol. Graph.* **8,** 52–56
30. DeLano, W. L. (2002) *The PyMOL Molecular Graphics System*, DeLano Scientific, San Carlos, CA
31. Nicholls, A., Sharp, K., and Honig, B. (1991) *Proteins Struct. Funct. Genet.* **11,** 281
32. Guther, M. L. S., and Ferguson, M. A. J. (1995) *EMBO J.* **14,** 3080–3093
33. Auld, D. S. (1995) *Methods Enzymol.* **248,** 228–242
34. Smith, T. K., Crossman, A., Paterson, M. J., Borissow, C. N., Brimacombe, J. S., and Ferguson, M. A. J. (2002) *J. Biol. Chem.* **277,** 37147–37153
35. Larson, K. S., and Auld, D. S. (1989) *Biochemistry* **28,** 9620–9625
36. Jackman, J. E., Raetz, C. R. H., and Fierke, C. A. (1998) *Biochemistry* **38,** 1902–1911
37. Waldo, G. S., Standish, B. M., Berendzen, J., and Terwillinger, T. C. (1999) *Nat. Biotech.* **17,** 691–695
38. Whittington, D. A., Rusche, K. M., Shin, H., Fierke, C. A., and Christianson, D. W. (2003) *Proc. Natl. Acad. Sci. U. S. A.* **100,** 8146–8150
39. White, R. J., Margolis, P. S., Trais, J., and Yuan, Z. (2003) *Curr. Opin. Pharmacol.* **3**, 502–507
40. Notredame, C., Higgins, D., and Heringa, J. (2000) *J. Mol. Biol.* **302,** 205–217